# A Study of Neodymium Magnet Replacement Technology for Electric Vehicle Traction Motor

**Kazuhiro Matsumura [1)] Shunji Oki [1)] Tomoaki Kaimori [1)] Ryosuke Minegishi [1)]**

*1) Powertrain and EV Electrical Technology Department, Nissan Motor Co., Ltd.,*
*560-2, Okatsukoku, Atsugi-shi, Kanagawa 243-0192, Japan*
*E-mail: kazuhiro-matsumura@mail.nissan.co.jp*

**ABSTRACT**: This paper studies the potential of using ferrite magnets as an alternative to neodymium magnets in motors for Electric Vehicles (EVs) to address the supply risks associated with neodymium magnets. While ferrite magnets offer a stable supply, their lower magnetic flux density reduces torque density. In general, since torque of Interior Permanent Magnet Synchronous Motor (IPMSM) using ferrite magnets primarily depend on reluctance torque, this study specifically focuses on enhancing reluctance torque while maintaining the same level of magnetic torque as the conventional type. Parametric study based on FEA was conducted to optimize electromagnetic circuit design for improving reluctance torque. The proposed U-bar type design effectively mitigates both stress and magnetic saturation by dividing the second layer of magnets into three segments and achieved an increased torque by 7% without sacrificing magnetic torque.

**KEY WORDS**: Electric vehicle, Ferrite magnet, IPMSM, Motor characteristics, Reluctance Torque

## 1. INTRODUCTION

In recent years, various measures have been implemented across different sectors to achieve carbon neutrality. In particular, the transportation sector, which accounts for a significant proportion of $CO_2$ emissions, aims to contribute to the reduction of greenhouse gas emissions by promoting electric vehicles. As a result, a diverse range of EVs has been manufactured year after year, leading to an increase in sales. However, the expansion of EVs poses risks, particularly concerning neodymium magnets (Nd magnet) used in traction motors. While they provide high torque density due to their high magnetic flux density, they contain rare earth elements, which can lead to potential price fluctuations and supply instability because mining locations for these elements are limited. Recently, studies on motors using neodymium magnets without heavy rare earth elements[(1)] or motors using ferrite magnets[(2)-(4)] was conducted as countermeasures to these risks.

The magnetic flux density of ferrite magnets is lower than that of neodymium magnets, which significantly impacts torque. Therefore, improving torque density is necessary to adapt ferrite magnets for use in traction motors. Most of the torque in ferrite magnet motors is provided by reluctance torque. Additionally, enhancing the magnetic torque requires increasing the volume of the magnets; however, significant improvements are limited due to stress constraints. Thus, this paper focuses on reluctance torque, which is the main component of ferrite motor torque.

Furthermore, it has been reported that rotors in which magnets are arranged in ∇ shape (referred to as ∇-type) demonstrate the best torque and power compared to other rotor shapes because the ∇-type utilizes reluctance torque most effectively[(5)]. Therefore, this paper explores configuration to enhance reluctance torque while maintaining the magnetic torque of the conventional ∇-type design as the same level, ultimately proposing a new electromagnetic circuit.

## 2. PERFORMANCE COMPARISON OF FERRITE AND Nd MAGNET

### 2.1. Comparison of magnet characteristics

The composition ratios of ferrite magnets are presented in Figure 1. Ferrite magnets are much less expensive than Nd magnets because their main component is iron oxide ($Fe_2O_3$). Moreover, the supply of ferrite magnets is stable. The primary metals used in ferrite magnets are iron (Fe) and strontium (Sr), which are readily available due to their global supply sources that do not depend on specific regions.

Regarding their magnetic properties, ferrite magnets have lower residual flux density and coercivity. Figure 2 presents a comparison of the magnetic characteristics of ferrite magnets and neodymium magnets. The magnetization of ferrite magnets is about one-fourth that of neodymium magnets, raising concerns about the impact on motor performance.

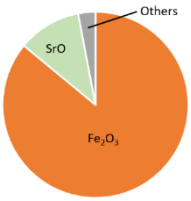


Fig. 1 Composition of ferrite magnet

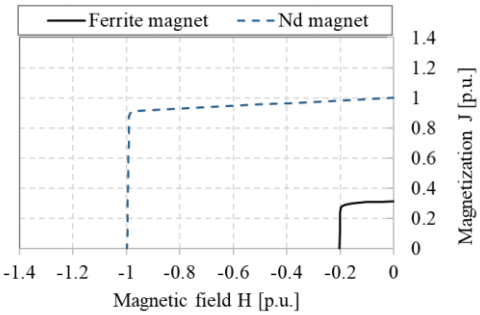


Fig. 2 Magnetic characteristics of ferrite magnet

### 2.2. Comparison of torque

To clarify the impact on torque when ferrite magnets are applied to motors, an analysis was conducted using an IPMSM that uses both neodymium magnets and ferrite magnets.

Table 1 shows the specifications of motor used for torque comparison and Figure 3 illustrates the cross-section of motor. As previously mentioned, the ∇-type demonstrates higher torque and power; therefore, a ∇-type rotor was utilized for this study. The motor's cross-section and active length were completely the same, but only the type of magnet was changed.

Figure 4 shows the difference in maximum torque under the same current and speed. When replaced with ferrite magnets, the maximum torque decreased, which is a 40% reduction. The breakdown of magnetic torque and reluctance torque is indicated by the color differences in Figure 4. It is shown that in ferrite magnet motors, the magnetic torque significantly decreases, and reluctance torque becomes the main component of torque. Improving magnetic torque requires increasing the magnetic flux, necessitating larger magnets in the magnetic circuit cross-section. However, this leads to excessive stress in the bridge section of the rotor core. Therefore, the constraints imposed by centrifugal forces become a bottleneck, making significant improvements in magnetic torque difficult to achieve. Thus, this paper focuses on reluctance torque, which is the main component of torque, and examines configurations for its improvement.

Table 1 Specification of torque comparison motor

| | | |
|---|---|---|
| Active length | 110 | [mm] |
| Rotor outer diameter | 121 | [mm] |
| Stator outer diameter | 176 | [mm] |
| Br of Nd magnet | 1.0 | [p.u.] |
| Br of Ferrite magnet | 0.3 | [p.u.] |

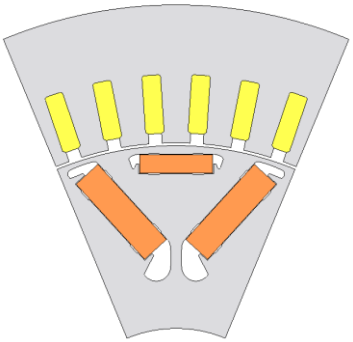

Fig. 3 Cross-section of prototype motor

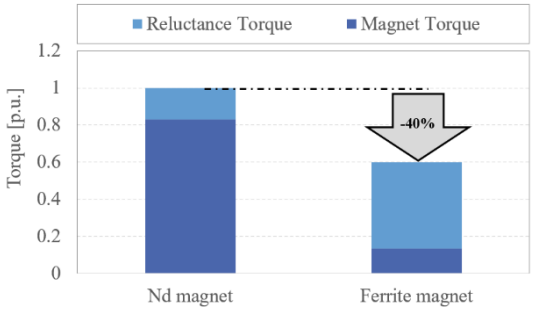


Fig. 4 Maximum torque comparison

## 3. SIMULATION ACCURACY AND CONDITIONS

### 3.1. FEA accuracy

Before starting the FEA optimization study, the accuracy of the torque provided by FEA is validated by comparing with measured value. Motor design shown in Figure 3 was fabricated, and torque measurement was performed.

The torque equations of the motor based on magnetic flux are shown in Equation (1) – (3), and the equations for inductance are presented in Equation (4), (5). Table 2 defines each parameter.

$$T = P_{\mathrm{n}}\{\Psi_{\mathrm{a}} I_{\mathrm{q}} - (L_{\mathrm{d}} - L_{\mathrm{q}}) I_{\mathrm{d}} I_{\mathrm{q}}\} \quad (1)$$

$$T_{\mathrm{m}} = P_{\mathrm{n}} \Psi_{\mathrm{a}} I_{\mathrm{q}} \quad (2)$$

$$T_{\mathrm{r}} = P_{\mathrm{n}} (L_{\mathrm{d}} - L_{\mathrm{q}}) I_{\mathrm{d}} I_{\mathrm{q}} \quad (3)$$

$$L_{\mathrm{d}} = \frac{\Psi_d - \Psi_a}{I_d} \quad (4)$$

$$L_{\mathrm{q}} = \frac{\Psi_q}{I_q} \quad (5)$$

$\Psi_a$ is the peak value of the coil linkage flux under no load ( no current) condition. In the load analysis with currents (*Id, Iq*), the component of the obtained coil linkage flux that is in phase with $\Psi_a$ is defined as $\Psi_d$, while the component of the coil linkage flux that is 90 degrees out of phase is defined as $\Psi_q$. Using the results from the FEA, each parameter is calculated, and finally, the torque is derived from Equation (1). For this FEA analysis, JMAG Designer Ver.23 was utilized.

Figure 5 shows the torque comparison between measurement and simulation results. Torque from FEA simulation in Figure 5 is obtained by subtracting the iron losses from the torque calculated using Equation (1). The difference in torque between the FEA and measurement is less than a few percent across all rotation ranges, confirming that the torque calculated by the FEA is accurate. Using this FEA methods, optimization study is conducted.

Table 2 Parameter for torque calculation

| Symbol | Meaning |
|---|---|
| T | Total torque |
| $T_m$ | Magnetic torque |
| $T_r$ | Reluctance torque |
| $\Psi_a$ | Magnet flux |
| $\Psi_d$ | d-axis flux |
| $\Psi_q$ | q-axis flux |
| $P_n$ | Number of pole pairs |
| $L_d$ | d-axis Inductance |
| $L_q$ | q-axis Inductance |
| $I_d$ | d-axis current |
| $I_q$ | q-axis current |

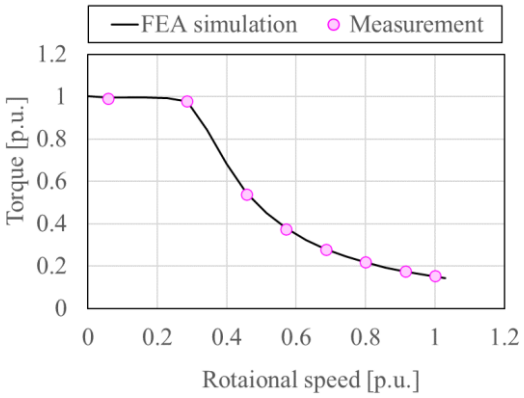


Fig. 5 Torque comparison between FEA and measurement

### 3.2. Simulation condition for FEA optimization

#### 3.2.1. Simulation flow and conditions

Firstly, model is created, and demagnetization analysis is conducted. Secondly, it is verified whether the model satisfies the demagnetization criteria; only those models that meet the criteria undergo centrifugal force analysis, no-load analysis, and load analysis, from which stress and each type of torque is obtained. Table 3 shows the simulation conditions. For demagnetization and load analysis, max current from Table 3 is adopted, while for centrifugal force analysis, max speed from Table 3 is adopted.

#### 3.2.2. Demagnetization analysis

One of the concerns about ferrite magnets is demagnetization. Therefore, demagnetization is considered as an objective function of the optimization analysis. Figure 6 shows the magnetization level contour from the demagnetization analysis. The demagnetization simulation is conducted under the worst temperature conditions, and the number of elements that are demagnetized in the magnets is counted from the contour in Figure 6, from which the demagnetization ratio is calculated. Designs that do not satisfy the demagnetization criteria are excluded from the optimization study.

Table 3 Simulation condition

| Condition | Value | Unit |
|---|---|---|
| Max Current | 240 | A |
| Max Speed | 18,500 | r/min |

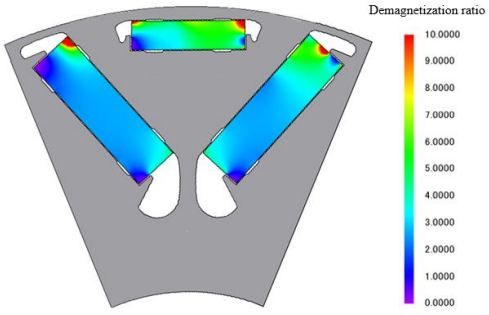


Fig. 6 Contour of demagnetization ratio

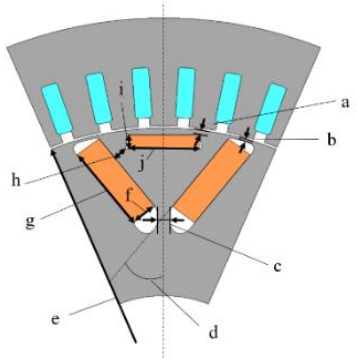


Fig. 7 Design parameter

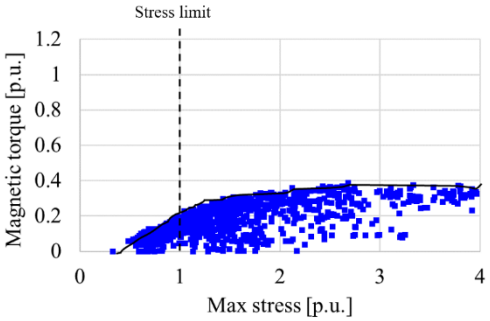


Fig. 8 Magnetic torque of ∇-type

Table 4 Parameter for optimization

| Symbol | Definition |
|---|---|
| a | Bridge of first layer magnet |
| b | Bridge of second layer magnet |
| c | Width of d-axis flux path (D_path) |
| d | Angle of Second layer magnet |
| e | Rotor diameter |
| f | Thickness of second layer magnet |
| g | Width of second layer magnet |
| h | Width of q-axis flux path (Q_path) |
| i | Thickness of first layer magnet |
| j | Width of first layer magnet |

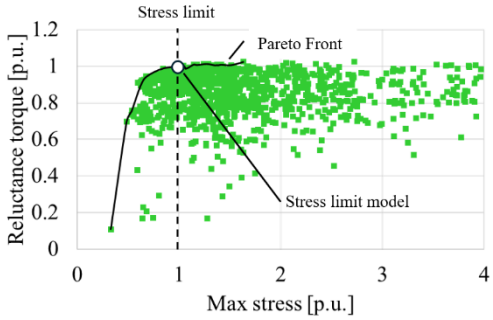


Fig. 9 Reluctance torque of ∇-type

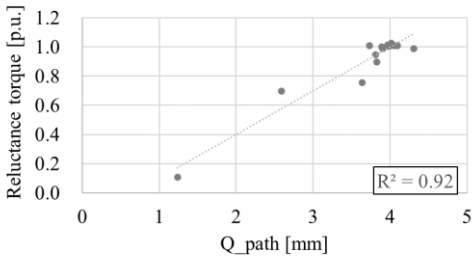


Fig. 10 Relationship between reluctance torque and Q_path

### 3.2.3. Design parameter

The optimization analysis of rotor core configurations was conducted using a genetic algorithm based on FEA, with the objective functions of maximizing torque and minimizing stress. The base design for the parametric study is the ∇-type configuration that uses ferrite magnets. Figure 7 shows the design parameter of ∇-type that have been modified during optimization study and definition of each parameter is represented in Table 4.

## 4. RELUCTANCE TORQUE ANALYSIS USING ∇-TYPE

### 4.1. Parameter optimization result

The FEA results are presented in Figure 8 and 9. Figure 8 illustrates the relationship between magnetic torque and stress, and Figure 9 shows the reluctance torque and stress. Magnetic torque and reluctance torque are computed by the Equation (2) and Equation (3). From the Pareto front graph in Figure 8, it can be observed that as the maximum magnetic torque increases, the stress also tends to rise.

As mentioned earlier, this is because as the volume of magnets increases, the magnetic flux and the magnetic torque increase, while at the same time, stress levels on the bridges become higher.

To analyze the details of reluctance torque, the Pareto Front in Figure 9 is focused on. Figure 10 illustrates the relationship between reluctance torque and the width of q-axis flux path (Q_path) of the design on the Pareto Front. The straight line in the graph represents an approximation, and it was found that there is a strong correlation. This suggests that as the Q_path is expanded, Lq increases, leading to an increase in reluctance torque.

To expand this Q_path, two methods can be considered:

1) Reducing the width of the first layer of magnets, and

2) Decreasing the angle of the second layer of magnets (making the magnets more upright).

These two approaches are examined based on the stress limit model seen in Figure 9.

### 4.2. Q_path Extension for reluctance torque improvement

#### 4.2.1. Width of first layer magnet

The reluctance torque when varying the width of the first layer magnets is shown in Figure 11, and relationship between magnet width and Ld, Lq are shown in Figure 12. From Figure 11, it can be observed that despite the reduction in the width of the magnets, the reluctance torque remains nearly constant. Figure 12 demonstrates that reducing the width of the magnets increases Lq, but Ld also increases by approximately the same amount. This is because when the width of the first layer magnets is reduced, the magnetic resistance of the d-axis also decreases, resulting in an increase in Ld. Therefore, while reducing the width of the magnets expands the Q_path and increases Lq, it also leads to an increase in Ld, which does not ultimately improve the reluctance torque. It can be inferred that it is essential to avoid reducing the dimensions of the first layer magnets in order to prevent an increase in Ld.

#### 4.2.2. Angle of the second layer magnets

To change the width of the Q_path, the angle of the second layer magnets was varied. Figure 13 shows the fixed points when changing the angle. All dimensions of the first layer magnets are fixed, and the edge of the second layer magnets and the width of D_path shown in Figure 13 are also fixed. By varying second magnet angle, the width of the Q_path is changed to investigate the sensitivity to reluctance torque.

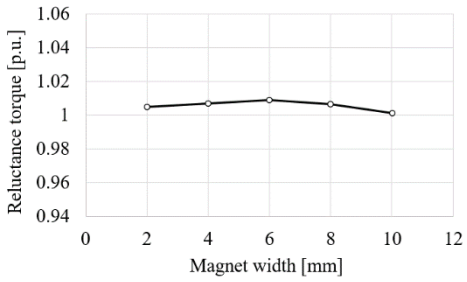


Fig. 11 Reluctance torque when magnet width changes

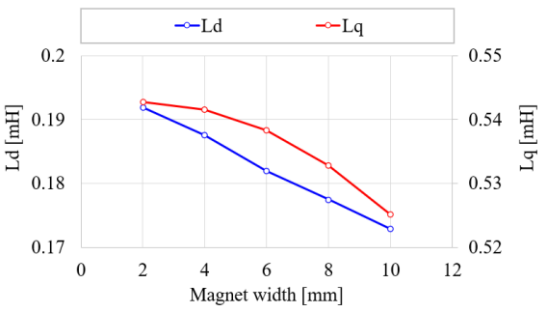


Fig. 12 Ld and Lq when magnet width changes

Figure 14 shows the relationship between Q_path and reluctance torque when the angle is changed, and Figure 15 presents each inductance. It can be observed that as the magnet angle decreases and the Q_path width increases, “Lq – Ld”, as well as the reluctance torque, increase. Figure 16 illustrates the magnetic flux density contour when the angle of the magnets is altered. When the angle becomes smaller and the Q_path is expanded, it is shown that the magnetic flux saturation between the magnets is mitigated. However, as the angle of the magnets becomes smaller and Q_path widens, the stress increases, as shown in Figure 17. This suggests that while decreasing the angle may widen the Q_path and improve reluctance torque, there are concerns about the resulting increase in stress.

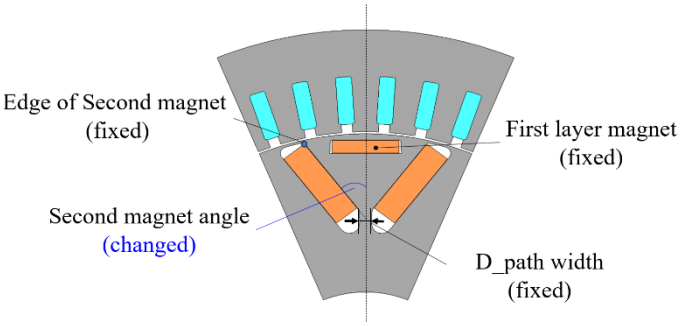


Fig. 13 Fixed point during angle change

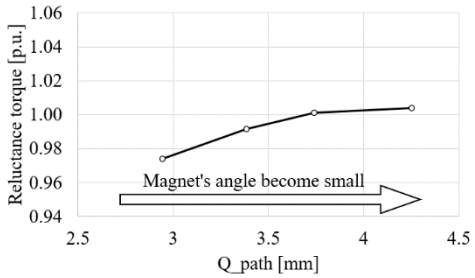


Fig. 14 Reluctance torque when magnet angle changes

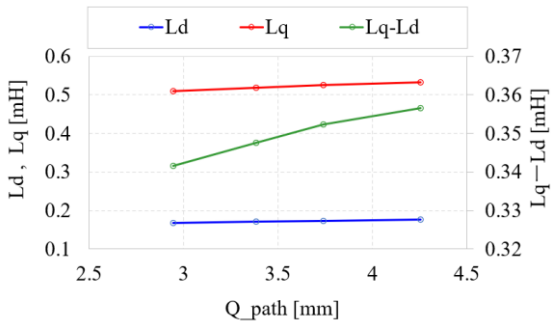


Fig. 15 Inductance when magnet angle changes

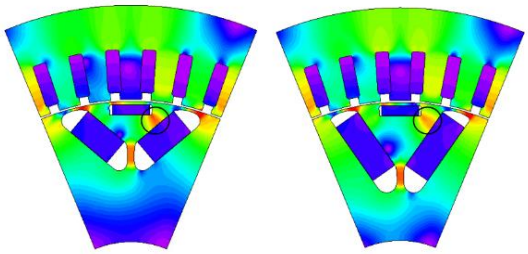

(a) Bigger angle model (b) Smaller angle model

Fig. 16 Flux density contour

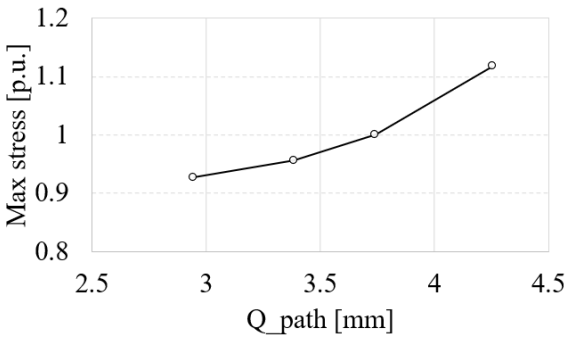


Fig. 17 Stress when magnet angle changes

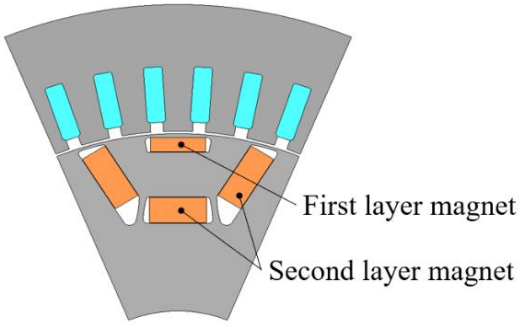


Fig. 18 Proposed rotor shape of Ubar-type

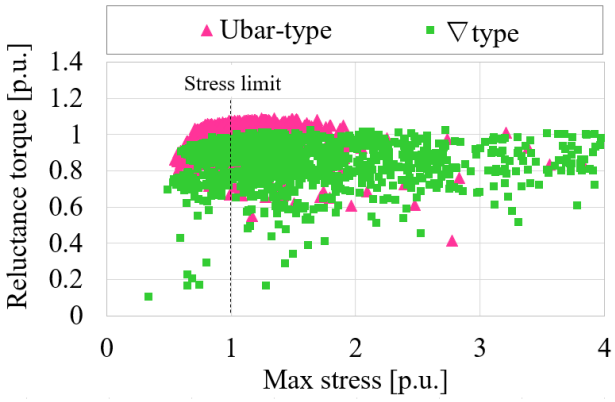


Fig. 19 Reluctance torque of Ubar-type

## 5. PROPOSED ROTOR DESIGN ANALYSIS

### 5.1. Proposed rotor geometry

It was found that the dimensions of the first layer magnets are important for reducing Ld, and that decreasing the angle of second layer magnets to widen the Q_path is essential for increasing reluctance torque. However, due to stress rebound, there is a limit to the improvement of torque in ∇-type design. Considering these factors, a new rotor design is proposed for further improvement of torque beyond the ∇-type.

Figure 18 shows the newly proposed rotor shape. In this shape, the magnets are arranged in Ubar-shape (referred to as Ubar-type). The second layer magnet is divided into 3 pieces and arranged in a U-shaped configuration. The first layer magnets are expected to help to reduce Ld in the same manner as ∇-type design. The second layer magnets are divided into three pieces, providing significant flexibility in their angles. This allows for a smaller angle of the second layer magnets, enabling the widening of Q_path. Furthermore, there are two bridges that support the centrifugal force, which mitigates stress concentration and enhances strength against centrifugal forces.

### 5.2. Parametric optimization result

The parametric optimization results for the Ubar-type and ∇-type are shown in Figure 19. It can be observed that the Ubar-type provides higher reluctance torque at the same stress compared to the ∇-type.

For further investigation, the models of ∇-type and Ubar-type motors that show the highest torque under the stress limits are compared. Figure 20 illustrates Ld and Lq, and Figure 21 displays the magnetic flux density contour plots for both types. From Figure 20, it can be observed that Lq has improved, while Ld remains nearly constant. Figure 21 indicates that the Ubar-type ensures sufficient Q_path distance, reducing magnetic saturation compared to the ∇-type. Consequently, the Ubar-type can increase "Lq-Ld".

Figure 22 illustrates the torque of both ∇-type and Ubar-type motors that shows highest torque under the stress limit. As a result of the improvement in Lq, the Ubar-type enhances reluctance torque while maintaining nearly the same magnetic torque as the ∇-type, resulting in an overall torque improvement of 7%.

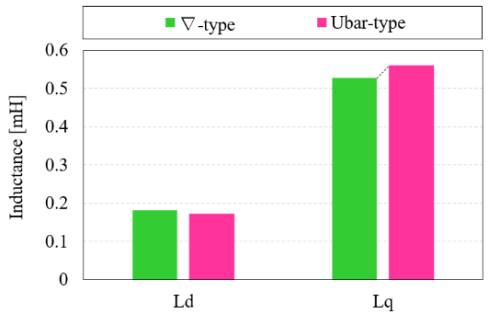


Fig. 20 Inductance of ∇-type and Ubar-type

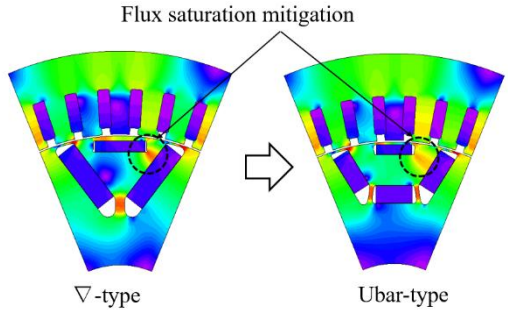


Fig. 21 Flux density contour of ∇-type and Ubar-type

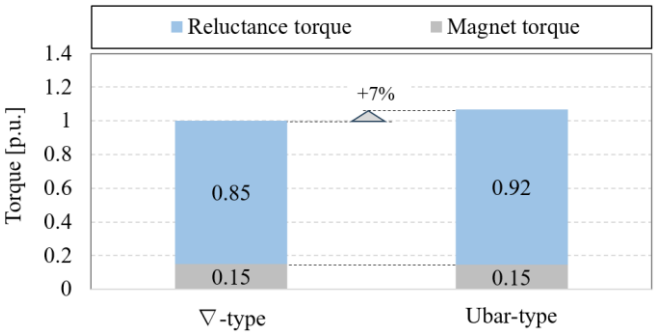


Fig. 22 Torque comparison of ∇-type and Ubar-type

## 6. CONCLUSIONS

The conclusions and contributions of this paper are summarized as follows:

- To mitigate material supply risks, a study was conducted on the application of ferrite magnets for traction motors.

- Shape optimization to improve reluctance torque with maintaining the magnetic torque of the conventional ∇-type was conducted, leading to the conclusion that ensuring sufficient dimensions of the first layer magnets and reducing angle of the second layer magnets are essential for enhancing reluctance torque.

- The U-bar type was proposed as a new electromagnetic circuit in which the second layer magnets are divided into 3 pieces, providing flexibility in the angle of the magnets and improving strength against centrifugal forces.

- The U-bar type mitigates magnetic saturation between the first and second layer magnets, resulting in a 7% improvement in total torque.

## REFERENCES

(1) Shingo Soma, Satoshi Fujishiro, Eiji Shirado : Research the Heavy-Rare-Earth-Free Motor for Hybrid Vehicle, Transactions of Society of Automotive Engineers of JapanVol.48, No.5, p. 1079-1083 (2017)

(2) Keun-Young Yoon, Byung-Il Kwon ,“Optimal Design of a New Interior Permanent Magnet Motor Using a Flared-Shape Arrangement of Ferrite Magnets”, IEEE Trans. Magn., vol. 52, Issue: 7, July. 2016.

(3) M. Kimiabeigi, J. D. Widmer et al. : High-Performance Low-Cost Electric Motor for Electric Vehicles Using Ferrite Magnets, IEEE Transactions on Industry Electronics, vol.63, Issue:1, Jan. 2016

(4) Sinisa Jurkovic, Khwaja Rahman, Nitin Patel, Peter Savagian : Next Generation Voltec Electric Machines; Design and Optimization for Performance and Rare-Earth Mitigation, SAE international 2015-01-1208

(5) Shunji Oki, Shigeaki Ishikawa, Takeshi Ikemi : Development of High-Power and High-Efficiency Motor for a Newly Developed Electric Vehicle, SAE international 2012-01-0342